Journal of Inorganic and Organometallic Polymers and Materials (2021) 31:1381–1394
https://doi.org/10.1007/s10904-020-01800-6

Synthesis, Characterization of [Co(BDC)(Phen)H_2O] and [Co(BDC)(DABCO)] MOFs, π..π Interactions, Hirshfeld Surface Analysis and Biological Activity

Amaravathi Chinthamreddy[1,2] · Raja Karreddula[3] · Gopi Krishna Pitchika[4] · Manabolu Surya SurendraBabu[1]

Received: 12 August 2020 / Accepted: 19 October 2020 / Published online: 30 October 2020

Abstract
Mixed-ligand [Co(BDC)(Phen)(H_2O)](**1**) and [Co(BDC)(DABCO)](**2**) MOFs were synthesized at 150 °C by solvothermal method. These MOFs analyzed by powder FT-IR, powder X-ray diffraction (PXRD), SEM and EDX and TGA-DTA analysis. The molecular structure confirmed by single-crystal XRD studies of **1** suggests a square planar structure with intermolecular π…π interaction between lateral 1,10-phenanthroline ring shows at a distance of 3.581 Å and 3.560 Å. Hirshfeld surfaces analysis of **1** mapped over d_{norm} displays extensive O–H/Co–O interactions and intermolecular H-bonding interactions. Antimicrobial activity of **1** is good comparatively with **2**, attributed to the release of cation metal ions easily and more extended period. Antioxidant studies against DPPH scavenging ability are shown a maximum of 48.62% inhibition by **1.** DNA cleavage activity of MOF **1** increases with the concentration increase.

Keywords Solvothermal method · Mixed ligand cobalt MOFs · 1,10–Phenanthroline · Antimicrobial activity · Hirshfeld surface analysis

1 Introduction

Recent years, increasing antibiotic resistance of pathogens bacterial contamination is one of the most challenging problems in many areas such as food storage, healthcare sector, and environmental fields is threatening public health [1, 2]. The application of metal complexes of phenanthroline and DABCO as antibacterial agents is well known, but the loss of activity in a short period is a significant drawback. At the same time, MOFs and nanoparticulate of metal/metal oxide systems have demonstrated significant long period antibacterial activity [3–5]. The advantage of MOFs, to act as a reservoir of metal ions and release ions steadily for an extended period. A stable, tunable structure and chemically active nature of MOFs are advantageous to control their interaction with active bacterial substances [6–9].

Only a few MOFs on antimicrobial activity is reported in the literature, such as silver-based metal–organoboron framework and 3-phosphobenzoate material acting as Ag^+ reservoir of silver ions and exhibited promising antimicrobial activity [10–13]. MOFs with a combination of drugs or antibiotics, offered a new approach to combat MDR bacterial strains to reduce the burden and increase the activity [12, 14]. Adding of biological activity moieties (i.e. 1,10-phenanthroline or DABCO) always advantages to improve the microbial activity [15]. Henceforth, present studies report on biological activity off mixed ligand [Co(BDC)(Phen)(H_2O)](**1**); [Co(BDC) (DABCO)](**2**) MOFs as valuable antimicrobial agents on *Saccharomyces cerevisiae, Bacillus subtilis* and *Escherichia coli* and good antioxidants and DNA cleavage activity.

✉ Manabolu Surya SurendraBabu
smanabol@gmail.com

[1] Department of Chemistry, School of Science, GITAM University, Telangana State, Hyderabad 502329, India

[2] Department of Chemistry, CMR Technical Campus, Hyderabad 501401, Telangana State, India

[3] Department of Chemistry, Rajeev Gandhi Memorial College of Engineering and Technology(Autonomous), Kurnool dist, Nandyal, Andhra Pradesh State, India

[4] Department of Zoology, Vikramshimapuri University, Nellore Dist, Kavali, Andhra Pradesh State, India

2 Materials and Methods

2.1 Materials

$Co(NO_3)_2.6H_2O$ 1,4-Benzenedicarboxylic acid (H_2BDC; purity > 99%), 1,10-phenanthroline (Phen) and 1,4-diazabicyclo [2.2.2] octane (DABCO), agar–agar, ethanol, Nutrient Broth (N.B.), 1,1-diphenyl-2-picryl-hydrazyl (DPPH) and Ascorbic acid was procured from Sigma Aldrich, and DMF is purchased from S.D. Fine (India). All the above chemicals were used, without further purification.

2.2 Synthesis of MOFs 1 and 2

The $Co(NO_3)_2.6H_2O$ (0.296 mg,1 mmol) and Phen (0.180 mg,1 mmol) or DABCO (0.198 mg, 1 mmol) dissolved in 10 ml of water and H_2BDC (0.111 mg, 0.69 mmol) dissolved in 10 ml of DMF, added to the above solution and stirred for 30 min at RT. The mixture solution is transferred into a 20 ml stainless steel autoclave and heated to 150 °C for 32 h. After 32 h brought to room temperature slowly and filtered to collect dark brown crystals and pale brownish ppt for **1** and **2** respectively.

2.3 Characterization

Rigaku automatic diffractometer (ULTIMA-IV,40 kV, 30MA) was used for Powder X-ray diffraction (XRD) experiments with monochromatic Cu k_α radiation. M/s. PerkinElmer G.X. spectrometer recorded FT-IR spectra with a scan range 4000–400 cm^{-1}. MOFs SEM images were taken on Electron Gun-cold cathode field emission (Hitachi S-4800) type. TG/DTA analysis was studied with the help of Netzch STA 449c Jupiter thermogravimetric analyzer heating the MOFs from 0 °C to 1000 °C under a constant N_2 flow (60 mL min^{-1}) at a rate of 10 °C min^{-1}.

Crystal **1** with suitable dimensions was mounted on a CryoLoop (Hampton Research Corp., at IIT Hyderabad) with a layer of light mineral oil and placed in a nitrogen stream at 150°K. All measurements were made on an Oxford Supernova X-Calibur Eos CCD detector with graphite-monochromated Cu-K_α (1.54184 Å) radiation, CrysAlisPro, Agilent Technologies, Version 1.171.35.19. The structures were solved by direct methods (SIR92) and refined on F2 by full-matrix least-squares using SHELXL-97. ORTEP-3 was used to draw the molecule.

2.4 Hirshfeld Surface and Void Analysis

Crystal Explorer17.5 generated Hirshfeld surfaces and 2D fingerprint plots [16] using single-crystal X-ray diffraction results. The normalized contact distance (d_{norm}) on color scale of − 0.55 Å (red) to 1.40 Å (blue) was mapped, while shape index in the range − 1 to 1 Å and curvedness in the range of − 4 to 4 for **1**. The normalized contact distance (d_{norm}) given by

$$d_{norm} = \frac{d_i - r_i^{vdW}}{r_i^{vdW}} + \frac{d_e - r_e^{vdW}}{r_e^{vdW}}$$

In the above equation, d_e and d_i represent the distances from any point to the nearest nucleus external and internal surface, respectively. r_i^{vdW} and r_e^{vdW} are the van der Waals radii of the atoms. The Hirshfeld surfaces are visualized as red colour due to the sum of d_i and d_e found shorter than the vdW of atoms(d_{norm} = −ve). The white colour displays an intermolecular distance equal to vdW (d_{norm} = 0) while blue colour display intermolecular distance longer than vdW (d_{norm} = + ve). d_i *vs* d_e is 2D fingerprint plot spots the different types of intermolecular interactions [17–20]

2.5 Biological Activity

2.5.1 Antimicrobiol Activity

Antimicrobial activity of **1** and **2** MOFs screened against *Bacillus subtilis* (gram + ve) (MTCC 441), *Escherichia coli* (gram −ve) (MTCC 443) and *Saccharomyces cerevisiae* (fungus) (MTCC 170) using the agar diffusion plate method and cup plate method [21] with Ciprofloxacin as control. A dilution series of **1** and **2** were prepared from a stock solution(test sample) of 1000 µg/ml in DMSO solvent and dilute it for further use. The agar media poured into the Petri dishes at R.T., wells or holes are made on solidified media by using sterile borer (8 mm diameter). The test samples 1 and 2 loaded with 2.5 µg/ml, 5.0 µg/ml, 10 µg/ml concentration and 0.25 µg—0.5 µg in agar diffusion method. Dilution plate count method is carried with **1** (10 to 50 ppm) on *Escherichia coli* (gram-negative) by placing directly onto the inoculated agar plate wells (agar diffusion method) and incubate at room temperature for 24 h (35 °C ± 2). After incubation, the diameter of zone inhibition is measured.

2.5.2 Release of Metal Test

The metal concentrations of **1** determined by using the 4-pyridylazoresocinol. The samples were taken out and dissolved in water; this suspension was sonicated and kept under stirring for a complete release of metal present in **1**. This dispersion was filtered by 0.2 µm membrane filter. The filtrate was mixed with 3 ml of 4-pyridylazoresocinol solution and 2 ml of 0.05 M borax buffer solution (maintain pH = 9) and measured the absorbance at 510 nm by using the Shimadzu U.V. spectrophotometer.

2.5.3 Antioxidant Activity of MOFs

The antioxidant activity of 1 and 2 was estimated using DPPH process [22]. The radical scavenging ability of **1** and **2** against DPPH (0.001 mM) with various concentration (20, 25, 30, 35 and 40 µl) was evaluated by adding, mixing and kept in the darkroom at R.T. for 30 min. These results compared with the standard reference against ascorbic (0.126 mM). DPPH activity evaluated by measuring absorbance at 517 nm with different volumes of **1** and **2** samples by the following expression

$$\text{DPPH Scavenging effect}(\%) = \frac{A_c - A_s}{A_c} \times 100$$

where A_c and A_s is the absorbance ascorbic acid (control) and test samples, respectively.

2.5.4 DNA Cleavage Activity

Plasmid pBR322 used for DNA cleavage activity using gel electrophoresis [23]. The Tris-buffer solution (0.05 M, pH 7.4), 0.1 µg/µL pBR322 DNA, and test sample **1** with concentration 0 µL, 0.5 µL, 1.0 µL, 1.5 µL and 2.0 µL in lanes 2–6 respectively. All mixtures incubated at 37 °C for 2 h. After 2 h, the incubated solutions added by loading buffer and carried electrophoresis for 45 min at 60 V by using an agarose gel. The gel was visualized and photographed under U.V.- light after completion (Scheme 1).

3 Results and Discussion

3.1 Characterization

FT-IR spectra of **1** and **2** MOFs shown in Fig. 1. The broad, strong peaks appeared at 1460 and 1550 cm^{-1} related to strong coupling of C–N of phenanthroline and C–C benzene ring stretching vibrations [24]. The peak at 2950 cm^{-1} in **2** assigned to aliphatic C-H asymmetric stretching band of DABCO. Absences of an intense peak at 1700 cm^{-1} proves -COOH groups in BDC are deprotonated in **1** and **2**, suggesting $–COO^-$ group in coordination with cobalt. The additional bands around 1650–1600 cm^{-1} and 1400–1380 cm^{-1} may be attributed to asymmetric vibrations of $-COO^-$ group and the benzene ring, while M–O stretching bands absorbed around 800–700 cm^{-1}.

MOF **1** crystallized in the triclinic phase and space group **P1** by solvothermal synthesis method. The asymmetric unit cell consists of two Co (II) ions coordinated

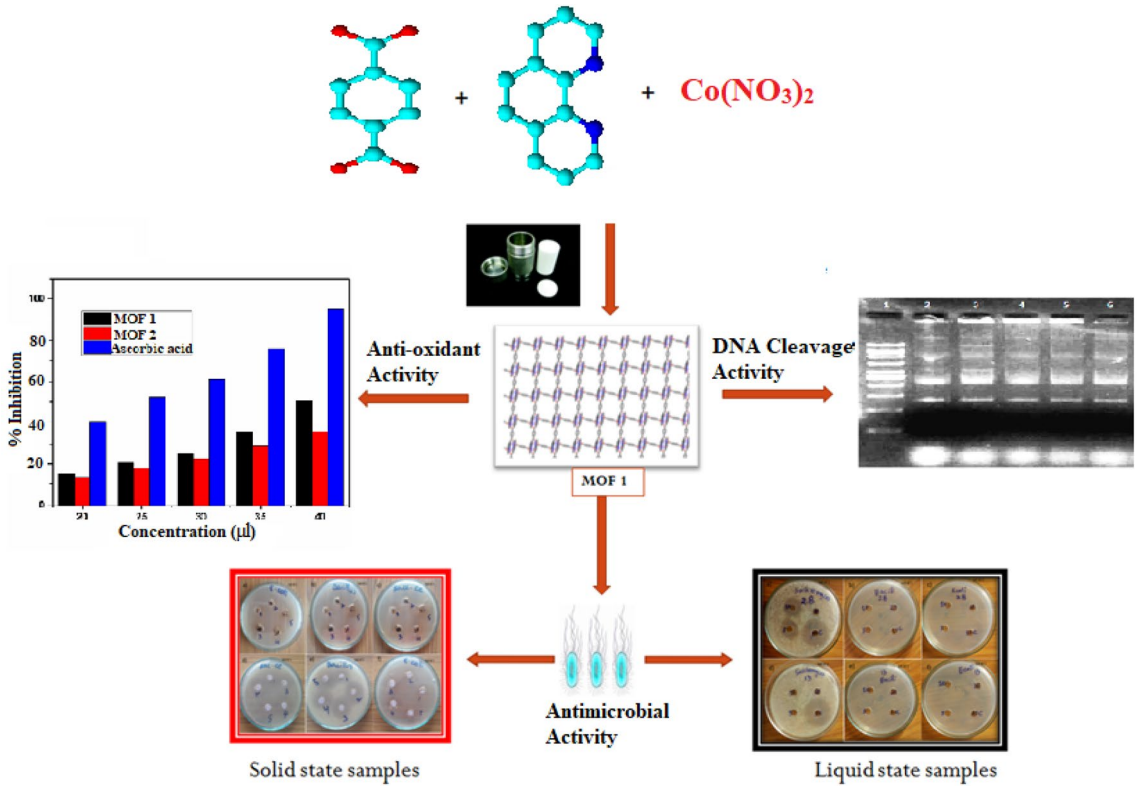

Scheme 1 Schematic representation of **1** and **2** hydrothermal synthesis and their biological activity

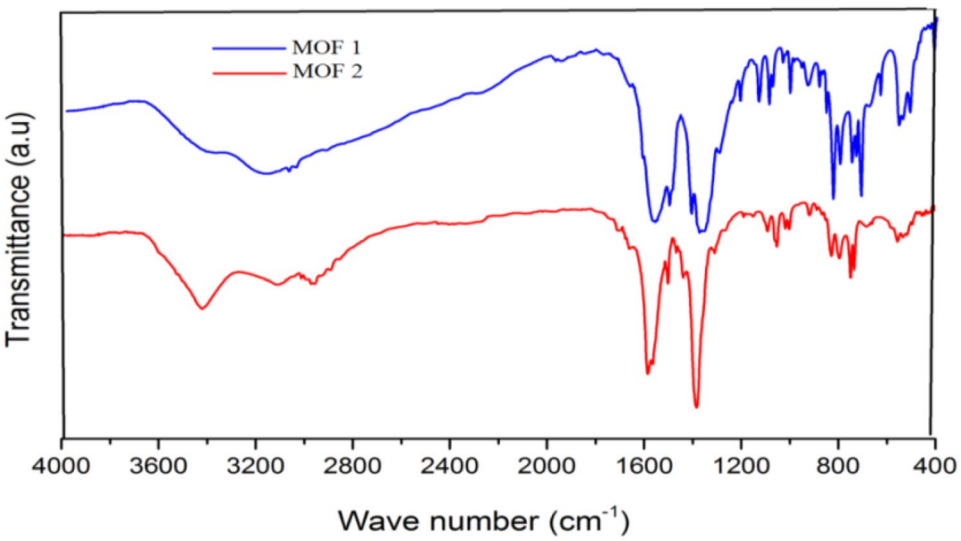

Fig. 1 F.T.- I.R. Spectra of MOF **1** and **2**

with two Phen molecules, two H_2O (one on each Co molecule) and two BDC ligands are shown in Fig. 2a The central cobalt metal ion coordinated by 2 N-atoms of Phen (the bond distance of Co—N, 2.139 and 2.132 Å); 2O-atoms of each BDC (Co—O, 2.049 Å) and a water molecule. These bond distances are well-matched with similar Phen complexes [25, 26]. Each BDC^{2-} ligand acts as a bridge between two cobalt atoms via two $–COO^-$ groups in a rare μ–anti-anti bridging chain structure. The helical cobalt chain connected with Co–Co distance 12.278 Å, and Co–Co-Co angle is 101. 08° orientation (Table 1).

It is observed moderately strong π-π stacking interactions with flanking Phen ligands (with face-face radius *ca.* 3.58 Å) from adjacent chains paired to form ladder-type layers. The ladder-type developed by Co-benzoic acid-Co and the two sides made by the π-π interactions (Fig. 2b). The dihedral angle of N···Co···N (Phen and Co) is 77.85°, and dihedral angle of O···Co···O (formed by 2 BDC and Cobalt) is 98.9°, this arrangement increases structural stability by reducing the steric hindrance. Further, bond angles and lengths given in Table 2.

Powder X-ray diffraction spectra of **2,** simulated and experimental are shown in Fig. 3. It is observed from the

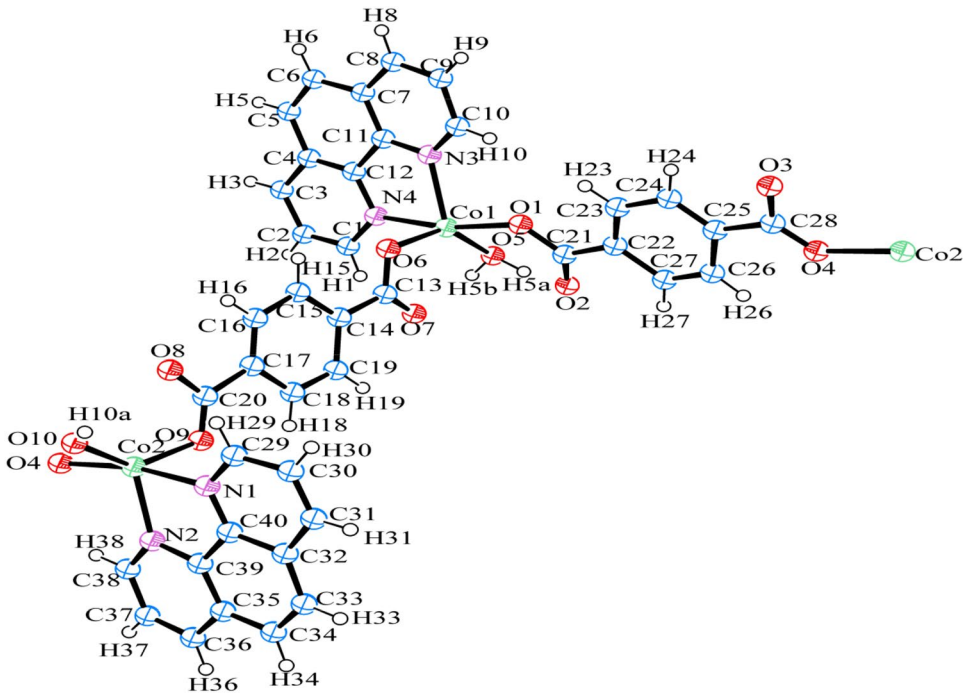

Fig. 2 **a** ORTEP view showing molecular structure of **1. b** The ladder-type structure formed by co-complex via π-π interactions

Fig. 2 (continued)

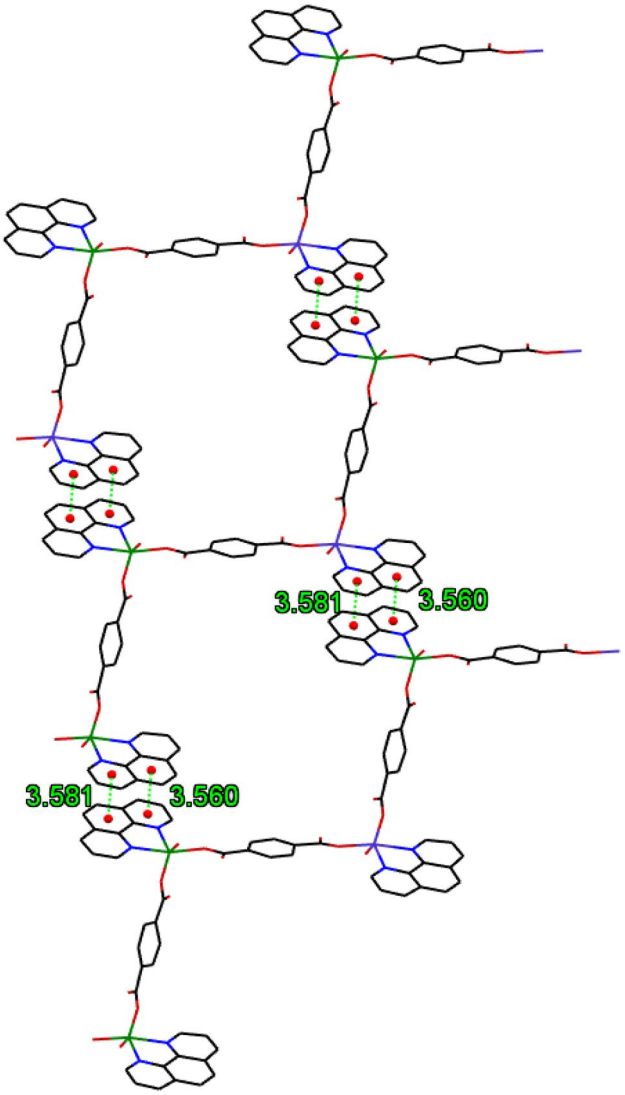

XRD pattern exhibits sharp, intense peaks below 10° (2θ values around 5.1, 8.1, 9.4, 11.3, 12.3, 16.2 and 18.7) indicating good crystalline nature of **2**. The overall XRD pattern shows that peaks of **2** match with reported data [26, 27].

Morphologies and elemental distribution of **1** and **2** analyzed by SEM—EDX studies. Figure 4 shows the SEM image of **1,** with a rough surface area, pores and heterogeneous crystals consisting of irregular shapes and sizes with an average particle thickness around 95 ± 12 µm. MOF **2** image in Fig. 5, shows well needle-shaped homogeneous particles with particle size in of 250-300 nm range. The elemental identification and atomic of samples were tested by the EDX spectrum, verifying the existence of elements in MOF **1** and **2**. EDX spectrum of MOF **1** and **2** is shown in Fig. 4e, Fig. 5e, in both spectrums presence of cobalt, is clear with weight % 21.04; 22.23 and atomic % 16.67; 20.91 respectively.

TG and DTA analysis of **1** and **2** are shown in Fig. 6. The T.G. curve recorded under N_2 atmosphere at temperatures ranging from 0 °C to 1000 °C. In Fig. 6a, MOF **1** show first weight loss at 180 °C due loss of water molecules coordinated to cobalt, also reflected in DTA curve by endothermic peak. A sudden fall in peak-I occurs in the range at 380 °C to 410 °C and a broad peak-II in a range 430–700 °C, corresponds to the decomposition of pillared BDC and Phen ligand. Peak I and II are shown as exothermic peaks in the DTA curve. Small endothermic peaks in Fig. 6b, at 180 °C and another at 220 °C of MOF **2** seen in the DTA curve**.** These peaks attributed to the loss of DMF solvent molecules. While slow fall in TGA curve up to 380 °C(range I), sudden fall 400–500 °C(range II), reflected in DTA curves as exothermic peaks due to the decomposition of BDC and DABCO ligands. TGA studies suggest these MOFs contain two different ligands and thermally stable up to 400 °C.

Table 1 Crystallographic data and structure refinement for **1**

Empirical formula	$C_{42}H_{29}Co_2N_4O_{10}$
Formula weight	826.52
Temperature	293°K
Wavelength	0.7107 Å
Crystal system,	Triclinic
space group	P1
Unit cell dimensions	a = 9.2651(6) Å α = 112.461(8) deg b = 10.4462(9) Å β = 94.889(6)deg c = 11.3303(10) Å γ = 113.980(7)deg
Volume	887.59(16)
Z, Calculated density, D_x(g, cm^{-3})	1, 1.546
Absorption coefficient	6.723 mm^{-1}
F(000)	422.0
crystal size	0.16 × 0.14 × 0.12 mm
h,k,l max	12,14,15
T_{min}, T_{max}	9516, 4758
R(reflections)	0.0507 (4031
wR2(reflections)	0.1672 (5233)
Absorption correction	multi-scan

Table 2 Bond Lengths [Å] and Angles [°] for **1**

Bond length /Bond angle		Bond length /Bond angle	
Co_1-O_1	1.99	C_{39}-N_{12}	1.32
Co_1-O_4	2.06	C_{32}-N_6	1.4
$Co_1 – O_9$	2.05	C_{45}-C_{32}	1.33
$Co_1 – N_6$	2.14	C_{30}- C_{32}	1.45
$Co_1 – N_{12}$	2.13	C_{30}- C_{36}	1.41
$Co_2 – N_5$	2.15	C_{39}- C_{47}	1.41
$Co_2 – N_{16}$	2.05	$C_{34} – N_5$	1.31
C_{30}- N_{12}	1.34	C_{44}- N_5	1.32
$O_1 – Co_1 – N_6$	166.7	$N_6 – Co_1 – N_{12}$	77.8
$O_1 – Co_1 – O_9$	99.5	$O_9 – Co_1 – N_{12}$	94.5
$O_1 – Co_1 – N_{12}$	92.4	$N_6 – Co_1 – O_4$	89.9
$O_9 – Co_1 – N_6$	90.3	$O_9 – Co_1 – O_4$	139.1
$O_1 – Co_1 – O_4$	88.6	$N_{12} – Co_1 – O_4$	125.4
$Co_2 – Co_1 – Co_3$	101.06		

As per the reports, these MOFs can exist in two forms (i) pillared square lattice. (solvothermal method) and (ii) Kagome net pillar structure (conventional). Based on the synthesis method, single-crystal analysis and PXRD results suggest these MOFs are pillared square lattice nature (Fig. 7) [28].

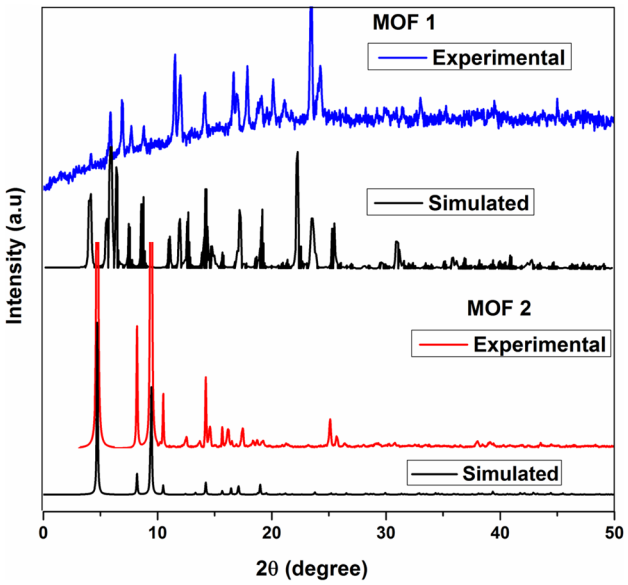

Fig. 3 Powder X-ray diffraction of **2** with simulated and experimental, respectively

3.2 Hirshfeld Surface Analysis

Crystal Explorer17.5 was used to generate Hirshfeld surfaces, and 2D fingerprint plot from crystal data of **1** are shown in Fig. 8**.** The Hirshfeld surfaces of **1** with different colour mapping in d_{norm}, shape index and three-dimensional curved shape reveal the different intermolecular interactions present in the crystal packing. Stable molecular packing in **1** is due to the close contact interactions, represented by red spots mapped over d_{norm} surfaces. The large red spots in **1** are due to strong intermolecular O···H interactions between -COO^- group of non-coordinated oxygen and H_2O molecule and small red colour spot are –COO^- and Co metal interactions as shown in Fig. 8a. The shape-index surface analysis of **1** show '*bow-tie*' pattern (Fig. 8b, black box in shape index,) in which red triangle represents C–C interactions present in *Phen* ring of the outer surface and blue triangle corresponds to C–C interaction of *Phen* ring inner surface. In Fig. 8c, Hirshfeld surfaces mapped over curvedness show a blue outline on Phen rings delineated on the flat surface indicated a stong π-π interaction. This π-π interaction is also reflected in 2D fingerprint plots with characteristic '*stacking kite*' pattern corresponding to C–C interactions (12.2%). The major intermolecular interaction analysed by 2-D fingerprint plots of **1** are shown in Fig. 9 as H···H (34.8%), H···C (22.5%), O···H (21.0%), C···C(12.2%), O···C (2.0%), and Co···O (1.5%) respectively [29–33] (Fig. 10).

Void surfaces analysis of **1** is picturized by crystal voids using crystal explorer17.5. The void surface is calculated by the isosurfaces of the promolecule density in the unit cell is less than a user-definable threshold. The volume of

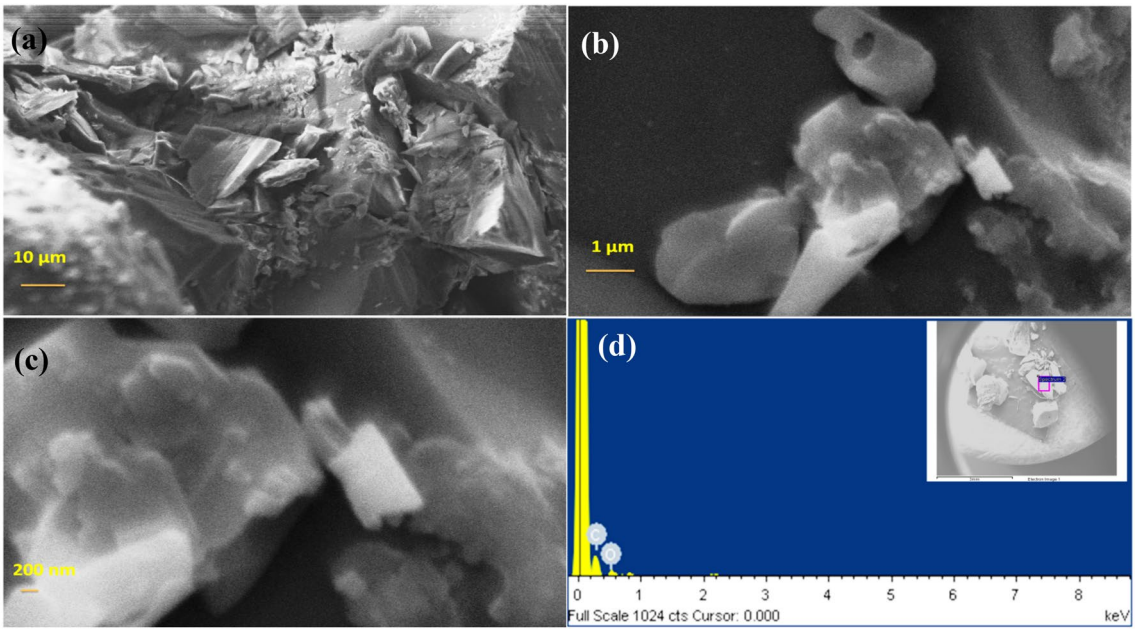

Fig. 4 SEM micrograph of **1** at **a** 10 µm, **b** 1 µm, **c** 200 nm, **d**, **e**, EDX spectrum of 1

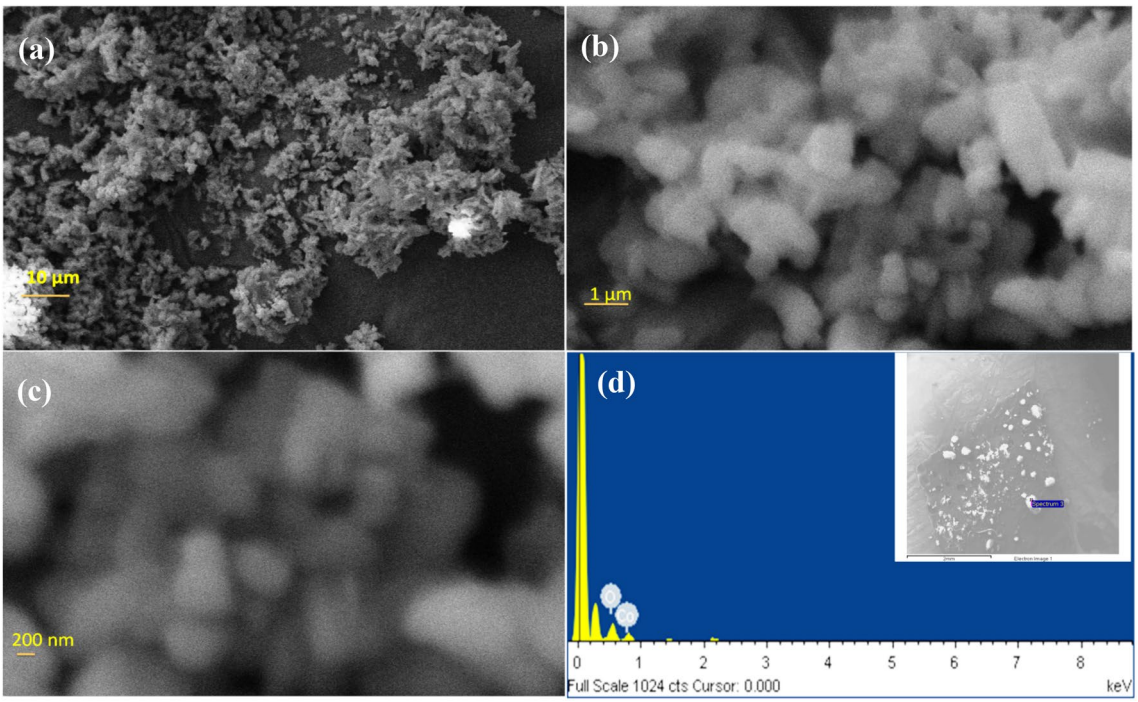

Fig. 5 SEM micrograph of **1 a** 10 µm, **b** 1 µm **c** 200 nm, **d**, **e** EDX spectrum of **2**

the void in **1** is 151.34 Å, and its surface area is 281.86 Å. The H-bonding measured in **1,** and **2** show a strong intermolecular H-bondings are present in **1**, between non-coordinated oxygen of carboxylic group in BDC and H_2O coordinated to another cobalt atom (HO-C = O….H–O-H). While in **2**, a very strong intra H-bonding is present, between carboxylic groups of BDC (HO-C = O····HO-C = O) (CCDC No: 661865) (Fig. 10).

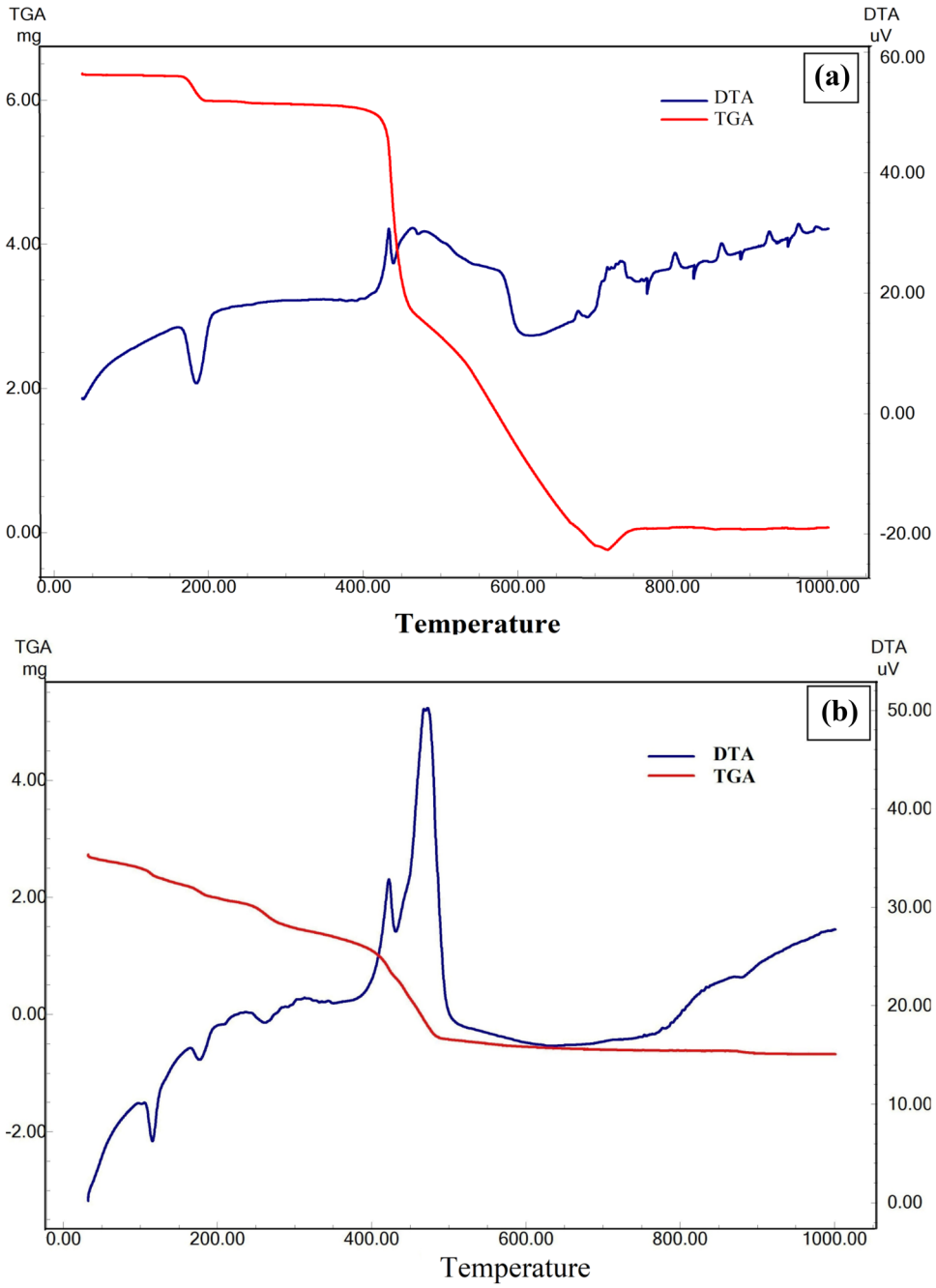

Fig. 6 **a** TG–DTA results of MOF **1** and **b** MOF **2**

3.3 Biological Activity

3.3.1 Antimicrobial Activity

The antimicrobial activity of **1** and **2** are evaluated using the agar diffusion plate count method and measuring the diameter of growth inhibition zones at different concentrations of the test solution. Microbiological activity is evaluated by; 2.5 µg/ml, 5.0 µg/ml and 10 µg/ml concentrations of **1** and **2** with control ciprofloxacin 10 µg/ml, add onto the inoculated agar plate Petri dish wells and incubate at R.T. for 24 h. From Fig. 11, it clearly is seen that **1** is active against saccharomyces, and the inhibition zone increase with the increase in concentration.

Further antimicrobial activity of **1** and **2** also evaluated with of 0.5 µg, 0.10 µg, 0.15 µg, 0.20 µg, 0.25 µg each solid MOFs placed directly onto the inoculated agar wells and incubating at R.T. for 24hrs. MOF **1** inhibited microbial growth more effectively with an increase in concentrations, while MOF **2** show good antibacterial activity, but the activity is less than **1** (Fig. 12).

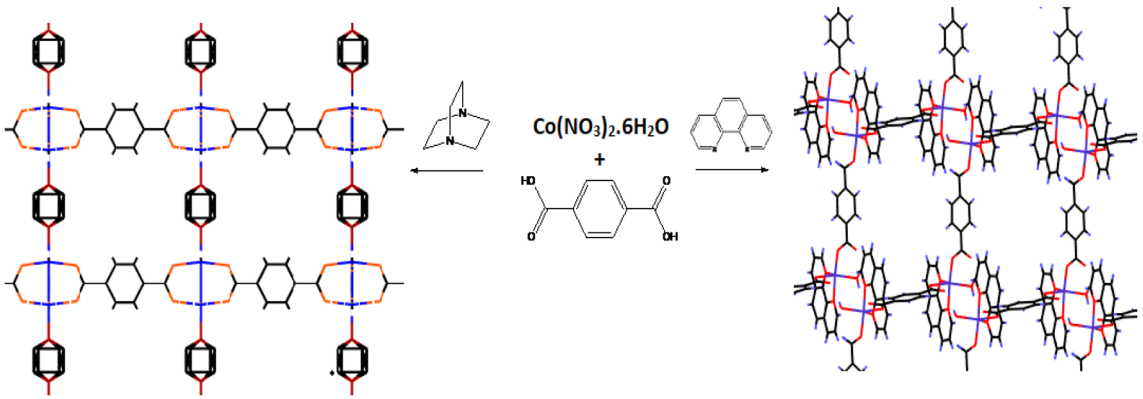

Fig. 7 Preferred Square lattice three-dimensional structures of the synthesized MOFs

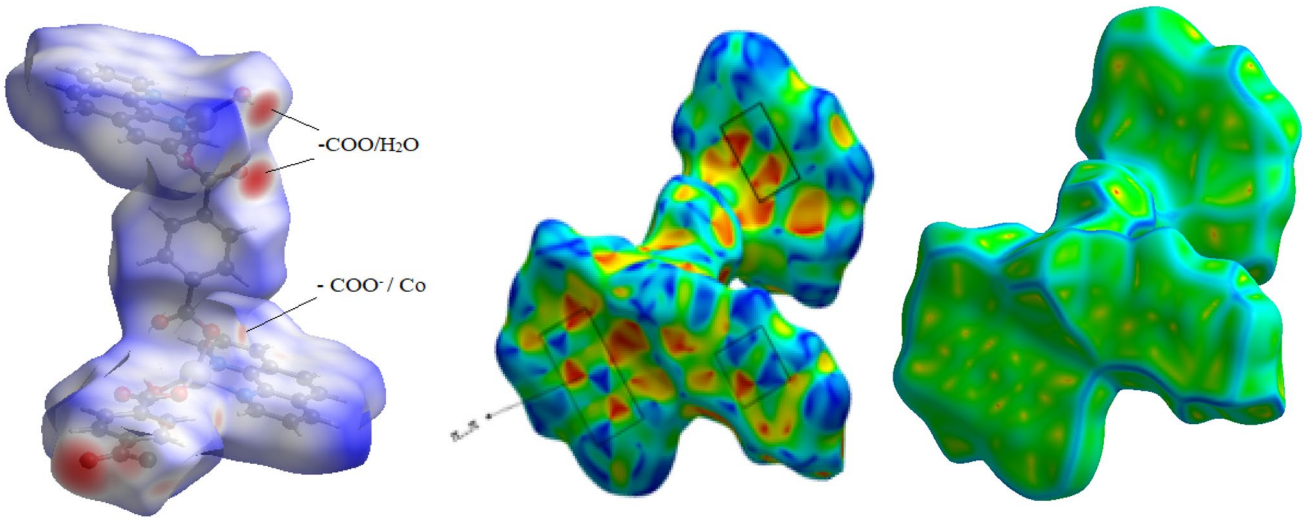

Fig. 8 Hirshfeld surfaces of **1** mapped with **a** d_{norm}, **b** shape index (middle) and **c** curvedness

The antimicrobial activity of **1** was also studied by the dilution plate count technique on *E.Coli.* by using nutrient agar media. In this culture, media contains SDA, nutrient agar with **1** at different concentrations (0 ppm(control), 10 ppm, 15 ppm, 20 ppm, 50 ppm, agar Petri dishes (Fig. 13). The bacteria inhibition appeared in all concentration; with an increase in concentration inhibition covers a large area due to the spreading of MOF particles. The higher antimicrobial activity of **1** may be attributed due to intermolecular H-bonding and phenanthroline ligand, while in **2** it involves stronger intramolecular H-bonding and coordination of DABCO between two cobalt atom which makes the release of metal difficult. Hence the cationic ion release ability of **1** is easier and faster than 2, makes **1** as ideal antimicrobial agent compares to **2** in antimicrobial inhibitions [34–37].

3.3.2 Anti-Oxidation Studies (Radical Scavenging Activity)

The antioxidant activity of 1 and 2 was evaluated using a reported DPPH assay method using ascorbic acid standard reference. DPPH act as a stable free radical, which in methanol, water, or ethanol [33]. The scavenging effect of DPPH carried by the addition of **1** and **2** with the change in **colour** is measured by UV–Vis spectra. The inhibition activity of **1** and **2** are compared with a reference standard of ascorbic acid, as shown in Fig. 14. The anti-oxidant activity was increased with the increased quantity of 1 and 2 (scavenging rate of **1** is 15.2, 20.6, 25.4,35.5, 50.7 and **2** is 13.5, 18.2, 22.4, 28.5 and 35.9% at concentrations as 20, 25, 30,35,40 µl respectively). The inhibition activity of 1 and 2 are compared with a reference standard of ascorbic acid, as shown in Fig. 14.

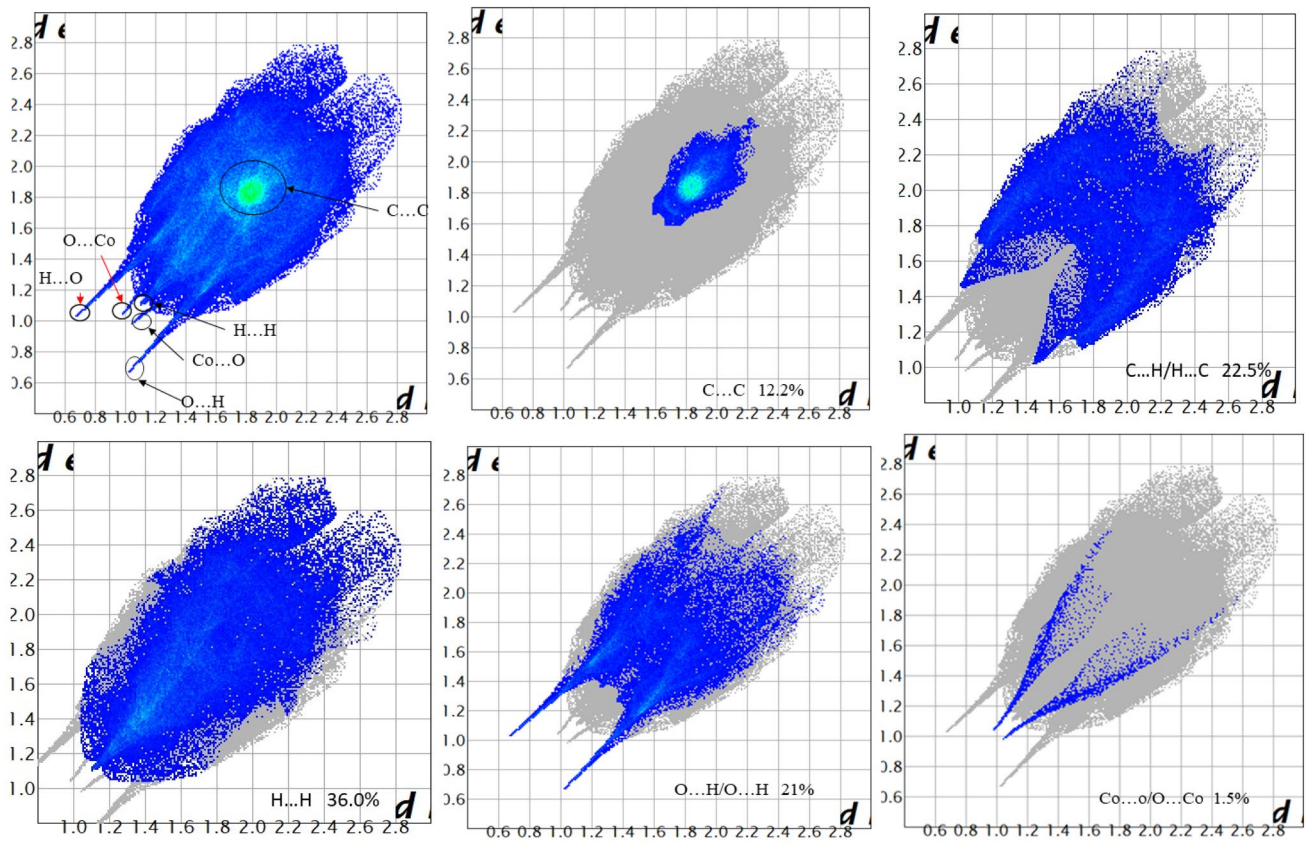

Fig. 9 2D Fingerprint plots, with all element interaction and resolved element interactions between C···C, C···H/C···H, H···H, O···H/H···O and Co···O/O···Co contacts in percentages

3.3.3 DNA Cleavage Activity

Cleavage activity of plasmid pBR322 DNA by **1** are investigated by gel electrophoresis using in Tris–HCl/NaCl buffer (50 mM and pH 8.0). The DNA cleavage is carried with control experiment without sample **1** in lane 2 and 1 µl, 2 µl, 3 µl, 5 µl of **1**(1 M) with increasing concentration in lane 3- 6 respectively (Fig. 15). It is clearly seen that with increasing concentration of **1,** the cleavage activity increases with the diminishing intensity of form I in lane 3–6 compared to From I in lane 2. The increasing intensity of Form II in lanes 3–6 is ascribed to the conversion Form-I to Form II, while the intensity of Form III is decreased compared to lane 2. MOF **1** cleaves Form I to Form II DNA, while Form III in lane 2 undergo shear cleavage appeared in lane 3–6 suggesting that **1** cleaves DNA moderately. Most of the metal complexes such as cobalt, copper, etc. cause DNA cleavage by classical electrostatic interactions with DNA, hence these interactions may be involved in DNA cleavage activity [38, 39].

4 Conclusions

Mixed ligand MOFs **1** and **2** are synthesized by the solvothermal method. X-ray crystal analysis reveals that **1** crystallizes in the monoclinic system, with space group **P1** each Co(II) ions coordinates with each Phen, BDC and a water molecule. SEM analysis of **1** shows a rough surface area with pores and heterogeneous crystals consisting of irregular shapes and **2** shows well needle-shaped homogeneous particles. TG–DTA suggest MOFs contain two different ligands are stable up to 400 °C. Hirshfeld surface and fingerprint plot **1** shows 'bow-tie' pattern shape-index surfaces, and also on shows 'stacking kite' pattern and carbon–carbon interactions are present, which comprises 12.2%. Indicates of π-π stacking interactions. MOF **1** show a significant antimicrobial activity to inhibit the growth of microorganisms for a longer period. MOF **1** is a potent antioxidant property with good radical scavenging activity(DPPH). The DNA cleavage activity of **1**

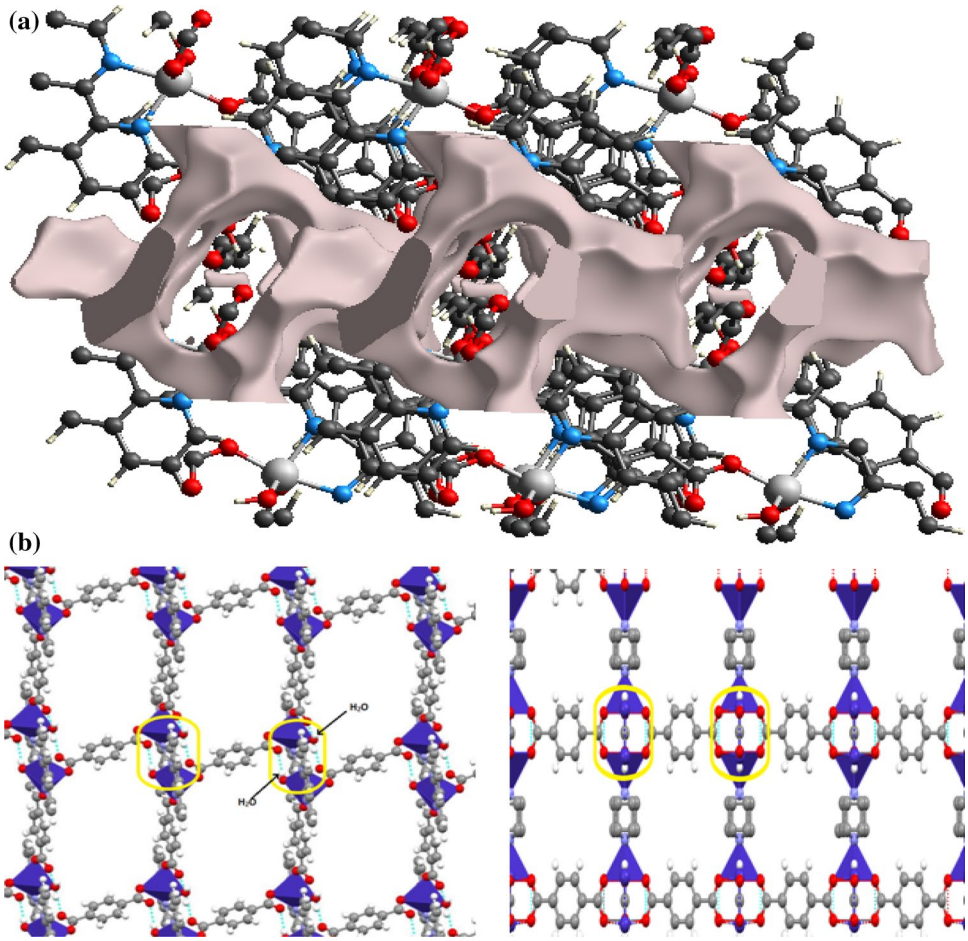

Fig. 10 Crystal void generate with isovalue of 0.002 e au^{-3}. **a** Intermolecular H…H bond in **1 b** Intramolecular H…H bond in **2**

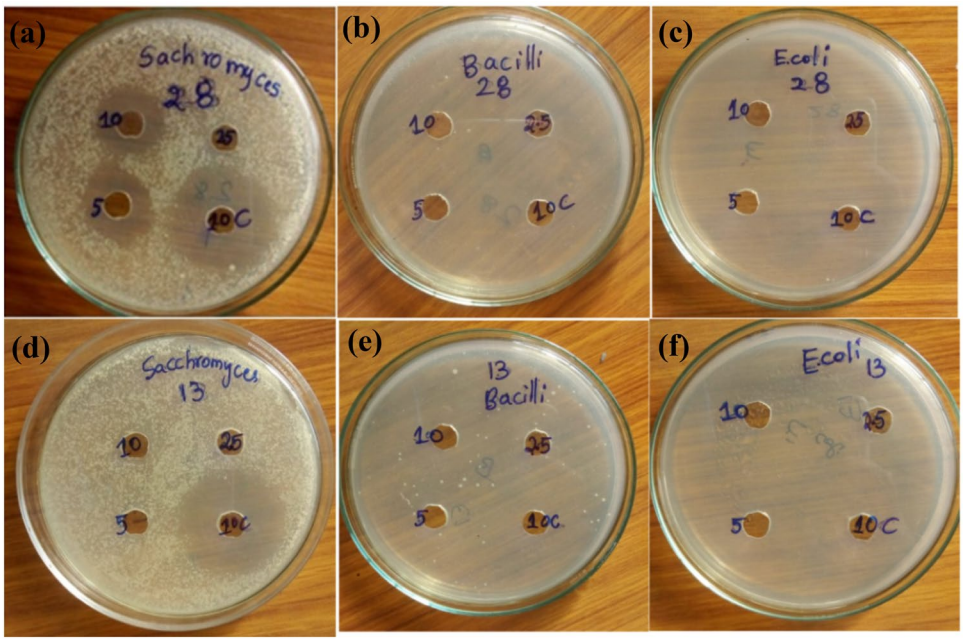

Fig. 11 Estimation antimicrobial activity by Agar plate diffusion experiment carried on S. Cerevisiae, *Bacillus and E. Coli* with MOF **1** and **2** in liquid form by 2.5 µg/ml, 5.0 µg/ml,10 µg/ml and control 10 µg/ml. Incubation conditions, R.T., 24 h

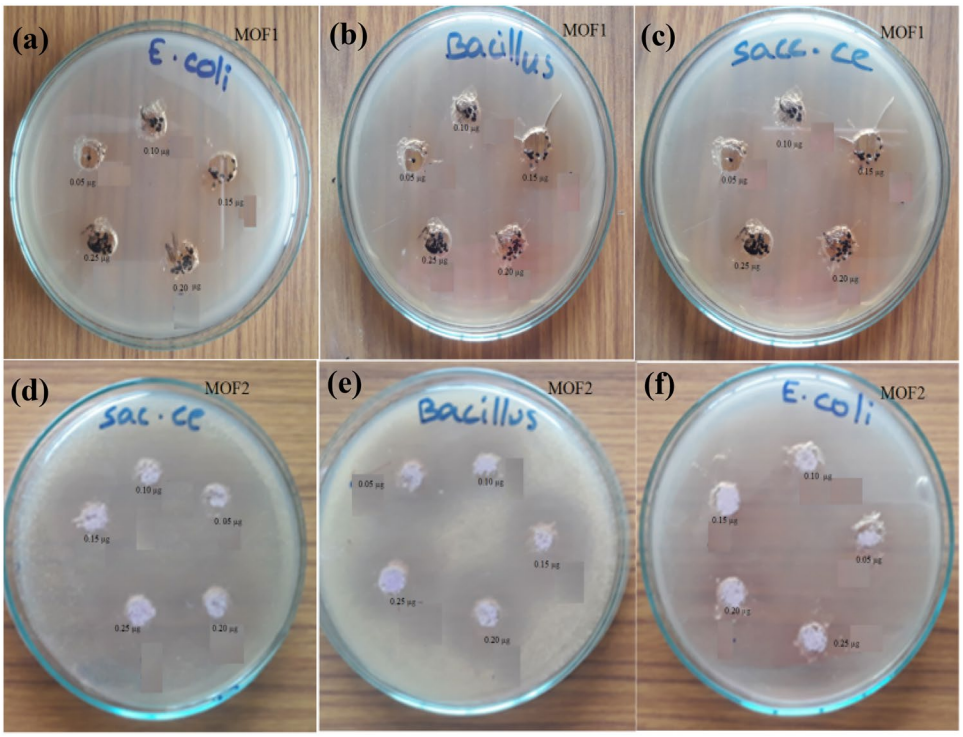

Fig. 12 Estimation of antibacterial and antimicrobial activity by Agar plate diffusion experiment carried on S. Cerevisiae, *Bacillus and E. Coli* with MOF **1**and 2 in solid form by 0.05 µg, 0.10 µg, 0.15 µg, 0.20 µg, 0.25 µg. Incubation conditions, 293°K, 24 h

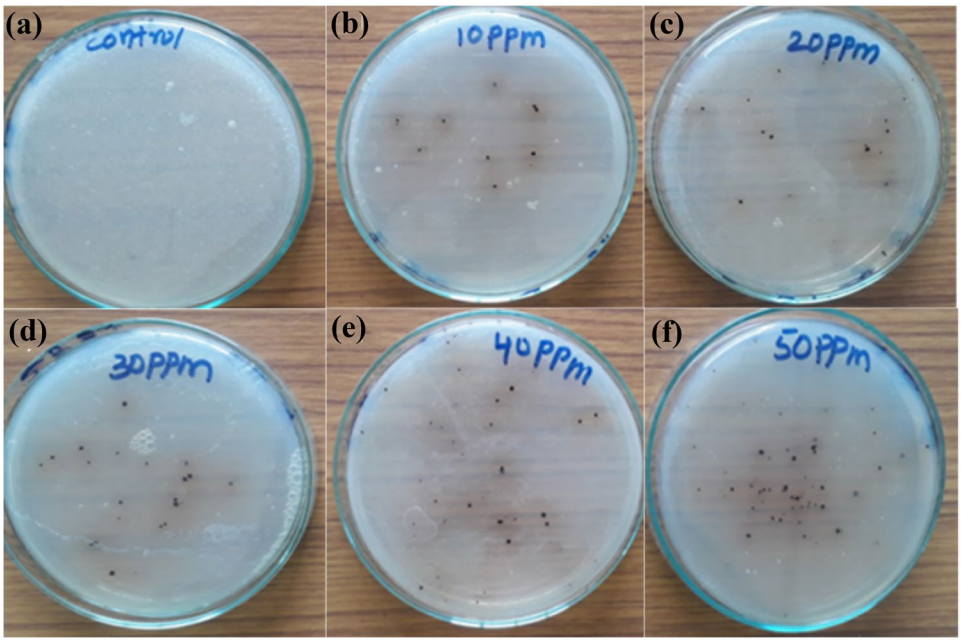

Fig. 13 Estimation of antibacterial activity by dilution plate technique carried on E.coli, with MOFs **1** in solid form by (1) control(without MOF1) (2) 10 ppm (3) 20 ppm (4) 30 ppm (5) 40 ppm (6) 50 ppm Incubation conditions, 293°K, 24 h

show enhanced DNA cleavage activity; hence MOF 1 is potential to be applied as the anti-nucleic agent.

Crystal Data: CCDC- 1,855,157 contains the crystallographic data of **1** can be obtained free of charge via the Cambridge Crystallographic Data Centre, 12, Union Road, Cambridge CB2IEZ, U.K. or via www.ccdc.cam.ac.uk.

https://www.ccdc.cam.ac.uk/mystructures/structuredetails/160b019c-3205-eb11-9694-00505695f620.

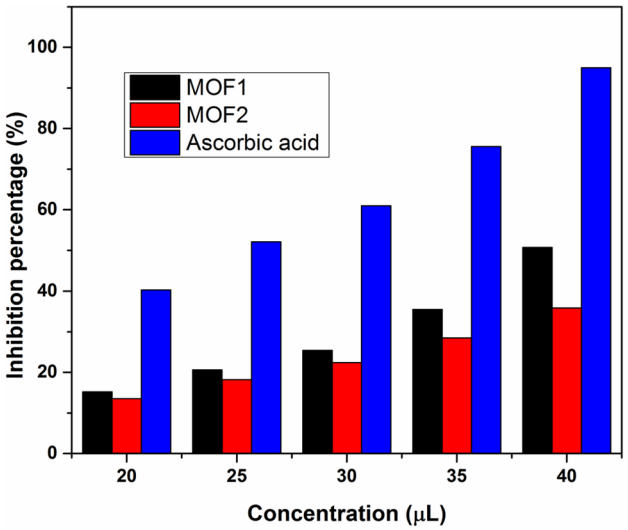

Fig. 14 The free radical scavenging activity of **1** and **2** through DPPH assay method

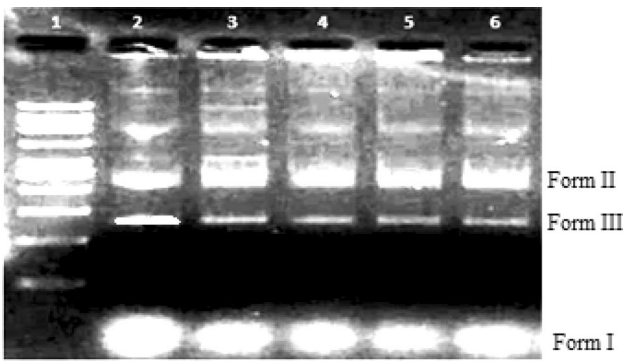

Fig. 15 Agarose gel (1%) showing the electrophoresis of 1 µl of (0.10 µg/ml) pBR 322 plasmid DNA, 2 µl of 0.1 M Tris–HCl (pH 8.0) buffer: 1 µl (1 M) 1 in DMF; 10 µl of sterilized distilled water were added, incubation at 37° C (2 h min): Lane 1: Marker; lane 2: DNA (control); lane 3: DNA + 1 (1 µl); lane 4: DNA + 1 (2 µl); lane 5: DNA + 1 (3 µl); lane 6: DNA + 1 (5 µl)

References

1. K.S. Ong, Y.L. Cheow, S.M. Lee, J. Adv. Res. **8**(4), 393–398 (2017)
2. A.C. McKinlay, R.E. Morris, P. Horcajada, G. Ferey, R. Gref, P. Couveur, C. Serre, Angew. Chem. Int. Ed. **49**, 6260–6266 (2010)
3. D.S.Y. Gaelle, D.M. Yufanyi, R. Jagan, M.O. Agwara, Cogent Chem. **2**, 1253201 (2016)
4. G.S. Anand, A. Sivanesan, M.R. Benzigar, G. Singh, A.I. Gopalan, A. Vijay Baskar, H. Ilbeygi, K. Ramadass, V. Kambala, A. Vinu, Bull. Chem. Soc. Jpn. **92**(1), 216–244 (2019)
5. A. Gupta, S. Mumtaz, C.H. Li, I. Hussain, V.M. Rotello, Chem. Soc. Rev. **48**, 415–427 (2019)
6. J. Chen, J. Zhu, S. Luo, X. Zhong, Chem. Pap. **74**(3), 859–866 (2020)
7. X. Wei, D. Xu, K. Ge, S. Qi, Y. Chen., (2020) J. Inorg. Organomet. Polym. **30(10)**: 3862–3868
8. X. Ren, C. Yang, L. Zhang, S. Li, S. Shi, R. Wang, X. Zhang, T. Yue, J. Sun, J. Wang, Nanoscale **11**, 11830–11838 (2019)
9. C. Gecgel, U.B. Simsek, M. Turabik, S. Ozdemir, J. Inorg. Organmet. Polym. **30**(3), 749–757 (2020)
10. M. Berchel, T. Le Gall, C. Denis, S. Le Hir, F. Quentel, C. Elleouet, T. Montier, J.M. Rueff, J.Y. Salaun, J.P. Haelters, G.B. Hix, New J. Chem. **35**, 1000–1003 (2011)
11. N. Bhardwaj, S.K. Pandey, J. Mehta, S.K. Bhardwaj, K.H. Kim, A. Deep, Toxicol. Res. **7**, 931–941 (2018)
12. Y. Liu, X. Xu, Q. Xia, G. Yuan, Q. He, Y. Cui, Chem. Comm. **46**, 2608–2610 (2010)
13. W. Zhuang, D. Yuan, J.R. Li, Z. Luo, H.C. Zhou, S. Bashir, J. Liu, Adv. Healthc. Mater. **1**, 225–238 (2012)
14. H. Nabipour, M.Hossaini Sadr, G. R. Bardajee J. Coord. Chem. **70**, 2771–2784 (2017)
15. J.A. Eremina, E.V. Lider, T.S. Sukhikh, L.S. Klyushova, M.L. Perepechaeva, D.G. Sheven, A.S. Berezin, A.Y. Grishanova, V.I. Potkin, Inorg. Chimica Acta. **510**, 119778 (2020)
16. J. Turner, J.J. McKinnon, S.K. Wolff, D.J. Grimwood, P.R. Spackman, D. Jayatilaka, M.A. Spackman, CrystalExplorer17, University of Western Australia, (2017).
17. F.L. Hirshfeld, Theoretica chimica act. **44**(2), 129–138 (1977)
18. M.A. Spackman, D. Jayatilaka Cryst. Eng. Comm. **11**, 19–32 (2009)
19. M.A. Spackman, J.J. McKinnon, Cryst. Eng. Comm. **4**, 378 (2002)
20. K.R. Fiebelkorn, S.A. Crawford, M.L. McElmeel, J.H. Jorgensen, J. Clin. Microbiol. **41**, 4740–4744 (2003)
21. A.B. Hanan, M.K. Zahran, E.E. Hossam, Int. J. Boil. Macromol. **91**, 208–219 (2016)
22. Y.K., Mohanta, S.K.Panda, R. Jayabalan, N. Sharma, Front. Mol. Biosci. **4,** 1–9 (2017).
23. S. Mustafa, B.U. Rao, M.S. Surendrababu, K.K. Raju, G.N. Rao, Chem. Biodiv. **12**, 1516–1534 (2015)
24. T.P. Gerasimova, S.A. Katsyuba, Dalton trans. **42**, 1787–1797 (2013)
25. M. Kariem, M. Yawer, H.N. Sheikh, J. Solid State Chem. **231**, 239–247 (2015)
26. N.C. Thacker, P. Ji, Z. Lin, A. Urban, W. Lin, Faraday discuss. **201**, 303–315 (2017)
27. L. Peng, S. Wu, X. Yang, J. Hu, X. Fu, Q. Huo, J. Guan, RSC advan. **6**, 72433–72438 (2016)
28. J.G. Medina, G.M. Gonzalez, L.P. Londono, S.P.H. Rivera, R. Fu, A.J.H. Maldonado, Microporous Mesoporous Mater. **212**, 8–17 (2015)
29. H. Wang, J. Getzschmann, I. Senkovska, S. Kaskel, Microporous Mesoporous Mater. **116**, 653–657 (2008)
30. X.Z. Shen, T. Zhang, S. Broderick, K. Rajan, Mol. Syst. Des. Eng. **3**, 826–838 (2018)
31. M. Małecka, E. Budzise, Cryst. Eng. Comm. **16**, 6654–6663 (2014)
32. G. Mahmoudi, A. Bauza, R.D. Antonio, G. Piotr, K. Werner, F. Antonio, Cryst. Eng. Comm. **18**, 102–112 (2016)
33. Y.K. Mohanta, S.K. Panda, R. Jayabalan, N. Sharma, Front. Mol. Biosci. **4**, 1–9 (2017)
34. M. Shen, F. Forghani, X. Kong, D. Liu, X. Ye, S. Chen, T. Ding, Compr. Rev. Food Sci. Food Saf. **19**(4), 1397–1419 (2020)
35. W. Zhou, S. Begum, Z. Wang, P. Krolla, D. Wagner, S. Bräse, C. Wöll, M. Tsotsalas, A.C.S. Appl, Mater. Interfaces **10**(2), 1528–1533 (2018)
36. K. Tabatabaeian, M. Simayee, A. Shojaie, F. Mashayekhi, M. Hadavi, J. Iran. Chem. Soc. **17**(11), 2987–2995 (2020)
37. P.L. Wang, Chem. Rev. **119**(18), 10638–10690 (2019)

38. H. Gopinathan, N. Komathi, M.N. Arumugham, Inorg. Chim. Acta **416**, 93 (2014)
39. S. Abdalla, A. Aghbari, M. Yahya, Eur. J. Chem. **5**, 410 (2014)